**Structural Engineering and Mechanics**, *Vol. 72, No. 6 (2019) 675-687*
DOI: https://doi.org/10.12989/sem.2019.72.6.675


# Sensitivity analysis of the plastic hinge region in the wall pier of reinforced concrete bridges

Ali Babaei[1a], Alireza Mortezaei*[2] and Hamidreza Salehian[2b]

[1]*Civil Engineering Department, Semnan Branch, Islamic Azad University, Semnan, Iran*
[2]*Seismic Geotechnical and High Performance Concrete Research Centre, Civil Engineering Department, Semnan Branch, Islamic Azad University, Semnan, Iran*

*(Received May 10, 2019, Revised July 27, 2019, Accepted August 3, 2019)*

**Abstract.** As the bridges are an integral part of the transportation network, their function as one of the most important vital arteries during an earthquake is fundamental. In a design point of view, the bridges piers, and in particular the wall piers, are considered as effective structural elements in the seismic response of bridge structures due to their cantilever performance. Owing to reduced seismic load during design procedure, the response of these structural components should be ductile. This ductile behavior has a direct and decisive correlation to the development of plastic hinge region at the base of the wall pier. Several international seismic design codes and guidelines have suggested special detailing to assure ductile response in this region. In this paper, the parameters which affect the length of plastic hinge region in the reinforced concrete bridge with wall piers were examined and the sensitivity of these parameters was evaluated on the length of the plastic hinge region. Sensitivity analysis was accomplished by independently variable parameters with one standard deviation away from their means. For this aim, the Monte Carlo simulation, tornado diagram analysis, and first order second moment method were used to determine the uncertainties associated with analysis parameters. The results showed that, among the considered design variables, the aspect ratio of the pier wall (length to width ratio) and axial load level were the most important design parameters in the plastic hinge region, while the yield strength of transverse reinforcements had the least effect on determining the length of this region.

**Keywords:** Sensitivity analysis; plastic hinge; wall pier; tornado diagram

## 1. Introduction

As a vital artery, bridges are important infrastructures whose function is determinant before, during, and after any earthquake. Each structure consists of two main components, known as the superstructure and the substructure. For bridges with bearing, all structural components that transfer the force from the bearings to the ground are called the substructure. Bridge piers, abutment, foundation, and piles are the members of the substructure. On the other hand, the superstructure includes deck, beams, and any member involved in the transfer of passing traffic. The bridge piers, as the support of girders, transmit loads from the superstructure to the foundation. Hence, these structural components are subjected to axial and shear loads as well as very large biaxial bending moment. One of the common types of bridge piers, widely used in the configuration of bridges, is the wall pier (Figure 1).

The experience of the past earthquakes has shown that the wall piers of bridges, designed according to the modern regulations with appropriate reinforcement details in the plastic hinge region (Figure 2), have generally had a fairly good performance during an earthquake (Murat 2015).

Due to the influence of lateral loads and depending on the direction of loading, these piers have different stiffness values in two directions. According to Road Safety Regulations (Manual No. 2-267) (RSM Code No 267, 2005) and due to strict traffic regulations and limitations, a significant increase in stiffness of the wall pier of the bridges is considered, which reduces the lateral displacements and rotations. In order to adapt to the lateral rotation constraints for the safe movement of trains, this value is between 1.5e-3 and 2.0e-3 radians. However, the high stiffness of the wall pier can enhance the ductility demand at lower levels of lateral displacement and cause concern over the seismic performance of the wall pier of the bridges, leading to significant reduction of the ductility indexes. Note that in the regulations for seismic design of road and rail bridges, response modification factor (R-factor) of the wall piers is R = 2 (Code No 463, 2008).

Within the framework of performance-based seismic design, an accurate assessment of the structural demand is required instead of a conservative estimate with simplified and ideal assumptions. In general, the robust design of bridges against earthquakes is based on the modal elastic analysis using a number of response spectra (Code No 463, 2008). However, most concrete bridges with wall piers are expected to have non-elastic responses during strong earthquakes accompanied by crack propagation, concrete crushing, as well as yielding, failure, or buckling of the reinforcement (Figure 3). Therefore, proper estimation and identification of the parameters affecting this region and their impact is of great importance (Mortezaei 2015).

*Corresponding author, Associate Professor
E-mail: a.mortezaei@semnaniau.ac.ir
[a] Ph.D. Candidate
[b] Assistant Professor



ISSN: 1225-4568 (Print), 1598-6217 (Online)

(a) (b)

Fig. 1 An example of a wall pier of reinforced concrete bridges

(a) (b)

Fig. 2 Seismic performance of the concrete bridge wall piers during the earthquake

Fig. 3 Some permanent damages on the Wu-Shi Bridge wall pier after the Chichi earthquake (Sung *et al*. 2009)

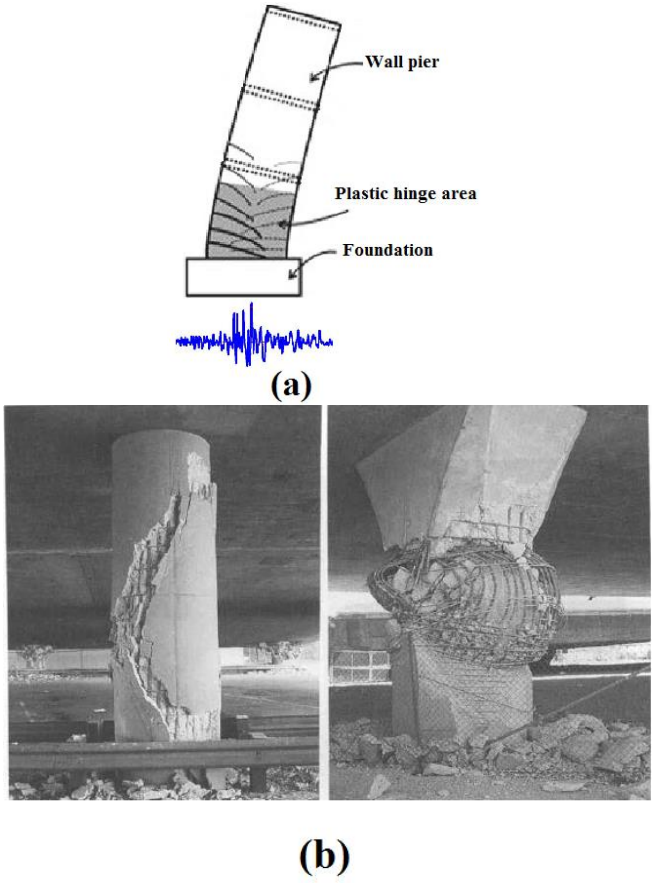


Fig. 4 (a) Schematic representation of the plastic hinge region, (b) Shear failure in the plastic hinge region in the San Fernando earthquake, 1971 (Alim 2014)

The present research is aiming to identify the key parameters affecting the length of plastic hinge region forms in the reinforced concrete bridge with wall piers through the sensitivity analysis in which three different approaches including the Monte Carlo simulation, tornado diagram analysis, and first order second moment method are considered for determining the uncertainties associated with analysis parameters.

## 2. Plastic hinge region

Reinforced concrete bridge piers are usually designed to resist against moderate to strong seismic events with considerable non-elastic deformation. These non-elastic deformations often associated with damages localized close to the pier connection to the foundation at the bottom regions of the bridge pier. The part of the pier during which non-elastic deformations occur is commonly known as the "critical plastic region", where a non-elastic flexural response is required throughout this region to dissipate seismic energy.

The nonlinear response of the plastic region affects the overall structural response of the bride. To assure the ductility of the plastic region, much higher percentage of transversal reinforcement is recommended for this region. Furthermore, additional lateral confinement along the critical plastic zone is recommended when seismic strengthening is aiming. Therefore, an accurate estimation of the length of the plastic region is essential for proper seismic design as well as improvement and retrofit designs.

The length of the plastic region represents a physical region in which the plastic deformation actually extends along the length of the reinforced concrete member (Figure 4a). On the other hand, the plastic hinge length is an equivalent term used in concentrated plasticity models to take into account inelastic deformations for determining the post-elastic deformations of wall piers and columns (Ghaderi Bafti *et al*. 2019).

The length of the plastic hinge is related to the length of the plastic region, since the length of the latter reflects the non-elastic deformation along the plastic hinge extending along the member due to bending which is known as the moment gradient component. In order to determine the extent of the plastic region, experimental tests on real scale are usually used. Many experimental relationships have been proposed to estimate the extent of the plastic region based on experimental results (Martezaei and Ronagh 2012), which include many different parameters, some of which are represented in Table 1.

Considering the variety of the intervening parameters adopted for determining the plastic hinge length, evaluation of the weight of the effect of these parameters in the length and profile of the plastic region is fundamental. The incorrect estimation of the length of the plastic region for the seismic design of reinforced concrete wall piers leads to inappropriate and inadequate reinforcement details for a ductile response and inversely affects the structural reliability of the structure to withstand considerable non-elastic deformation before the failure.

Seismic design guidelines require special reinforcement details and special confinement in the plastic regions of reinforced concrete wall pier in order to ensure a stable and ductile response. The ACI code (ACI 318, 2014) and Eurocode 8 (2004) define the length of the critical region ($l_0$ in the American Concrete Regulation and $l_{cr}$ in the European Code) in the columns of the ductile moment frames as follows, where the largest value of three quantities are: (a) the maximum dimension of the cross-section, (b) one sixth of net span, and (c) 450 mm.

According to the Canadian standard (CAN/CSA-A23.3-04, 2004), for the axial load ratio $(P/f_c^{'}.Ag)$ less than 0.5, the plastic region length for special reinforcement, isthe maximum value of (a) 1.5 times the largest dimension of the cross-section and (b) one sixth of the net span length.

The AASHTO seismic design instructions (AASHTO, 2011) define the length of the plastic region at the bridge pier as the largest values of three quantities: (a) 1.5 times the cross-section along the bending direction; (b) the length of the region where the demand moment is above 75% of the plastic moment; and (c) the length of the analytical plastic hinge length.

The Caltrans Instruction (Caltrans 2013) has compiled a ductile response for the plastic hinge region similar to the recommendations of the AASHTO instruction. The only exception is the last criterion, instead of which the criterion "a quarter of the distance from the maximum moment position to the turning point of bending" is included.

Table 1 Some expressions for the calculation of plastic hinge length

| Researchers | Expression |
|---|---|
| Baker | $l_p = k_1\, k_2\, k_3 \left(\frac{z}{d}\right)^{0.25} d$ |
| Baker & Amarakone | $l_p = 0.8\, k_1\, k_3 \left(\frac{z}{d}\right) c$ |
| Mattock | $l_p = \frac{d}{2}\left[1+\left(1.14\sqrt{\frac{z}{d}}-1\right)\left\{1-\left(\frac{q-q'}{q_b}\right)\sqrt{\frac{d}{16.2}}\right\}\right]$ |
| Corley | $l_p = 0.5\, d + 0.2\sqrt{d}\left(\frac{z}{d}\right)$ |
| Sawyer | $l_p = 0.25d + 0.075z$ |
| Park *et al*. | $l_p = 0.42h$ |
| Priestley and Park | $l_p = 0.08L + 6d_b$ |
| Riva and Cohn | From cracking to yielding limit state<br>$\frac{l_p}{z} = \left(A - \frac{B}{800\,\omega}\right)\left(\frac{\phi_p}{\phi_{py}}\right)^{\left(\frac{c}{80\omega}\right)}\left(\frac{b'}{b_w}\right)^{-\left(\frac{D}{640\omega^2}\right)} f(\gamma)$<br>From yielding to reinforcement strain hardening:<br>$\frac{l_p}{z} = \left(\frac{l_p}{z}\right) y \left(\frac{\phi_p}{\phi_{py}}\right)^{-(0.9-0.8\gamma)}$<br>Ultimate limit state<br>$\frac{l_p}{z} = \left(\frac{E}{100} + \frac{F}{1000}\frac{\phi_{pu}}{\phi_{py}}\right)\left(\frac{b}{b_w}\right)^G$ |
| Paulay and Priestley | $l_p = 0.08L + 0.15 d_b f_y$ $(f_y \text{ in ksi})$<br>$l_p = 0.08L + 0.022 d_b f_y$ $(f_y \text{ in MPa})$ |
| Sheikh and Khoury | $l_p = h$ |
| Berry *et al*. | $l_p = 0.05L + \frac{0.1 f_y d_b}{\sqrt{f_c'}}$ $(MPa)$<br>$l_p = 0.05L + \frac{0.008 f_y d_b}{\sqrt{f_c'}}$ $(psi)$ |
| Bae and Bayrak | $\frac{l_p}{h} = \left[0.3\left(\frac{P}{P_0}\right) + 3\left(\frac{A_s}{A_g}\right) - 0.1\right]\left(\frac{L}{h}\right) + 0.25 \geq 0.25$ |
| Mortezaei | $\frac{l_p}{h} = 0.80\left[1+0.40\frac{P}{P_0}\right]\left(\frac{H}{h}\right)^{0.2} k$ for $P/P_0 > 0.2$<br>$\frac{l_p}{h} = 0.50$ for $0 < P/P_0 \leq 0.2$ |

Note: $A_g$= gross area of concrete section; $A_s$=area of tension reinforcement; $d$ =effective depth of beam or column; $d_b$=diameter of longitudinal reinforcement; $E_c$=Young modulus of concrete; $f'_c$=concrete compressive strength; $f_y$= yielding stress of reinforcement; $h$ =overall depth of beam or column ;$H$ =overall height of column; $P$=applied axial force; $P_0$=$0.85f'_c(A_g-A_s)+f_yA_s$ = nominal axial load capacity as per ACI 318 (2014);$L$ = overall length of beam; $z$ =distance from critical section to point of contraflexure; $\phi$ = sectional curvature; $b_w$ = web width; A, B, C, D, E, F, G and f($\gamma$) constants depend on the bending moment distribution

Table 2 Description of axial load level, reinforcing scheme and material properties in the test program

| $\frac{P}{P_0}$ | Transverse reinforcement | | | | Longitudinal reinforcement | | | $f_c'$ (MPa) | Dimensions (mm×mm) |
|---|---|---|---|---|---|---|---|---|---|
| | $f_{ys}$ (MPa) | $\rho$ (%) | step (mm) | diameter (mm) | $f_y$ (MPa) | $\rho$ (%) | diameter (mm) | | |
| 0.5 | 400 | 1.28 | 90 | 10 | 470 | 1.62 | 13 | 23.5 | 180×1250 |

The New Zealand Standard (NZS 3101, 2006) and the European Rules for Bridges (Eurocode 8, 2005) propose the length with ductile details equal to the maximum between the following values: (a) the cross-section dimension along the bending frame; and (b) the length of the region along which the design moment is larger than 80% of base moment for $(P/f_c^{'}.Ag) < 0.25$, which is often the maximum axial load level in bridge piers.

In the present research work, 17 parameters are considered which, relying on the literature, may affect the length of plastic hinge forms inthe structural elements including beams, columns, shear walls, and frames. These parameters are summarized in the following:

(1) Axial load level $(P/P_0)$; (2) pier wall aspect ratio $\left({}^{H}/_{L}\right)$; (3) concrete compressive strength $(f_c)$; (4) ultimate compressive strain of concrete $(\varepsilon_{c_o})$; (5) concrete tensile strength $(f_t)$; (6) maximum tensile strain of concrete $(\varepsilon_t)$; (7) modulus of elasticity of concrete $(E_c)$; (8) yield strength of longitudinal steel $(f_{yL})$; (9) transverse steel yield strength $(f_{ys})$; (10) longitudinal steel ratio $(\rho_{sL})$; (11) transverse steel ratio $(\rho_{sh})$; (12) ultimate longitudinal steel strain $(\varepsilon_{ul})$; (13) ultimate strength of longitudinal steel $(f_{ul})$; (14) modulus of elasticity of steel $(E_s)$; (15) ultimate strain of transverse steel $(\varepsilon_{uh})$; (16) longitudinal steel diameter $(d_{sl})$; and (17) transverse steel diameter $(d_{sh})$. These parameters capture the material properties of concrete and steel,structural geometry, and load level.

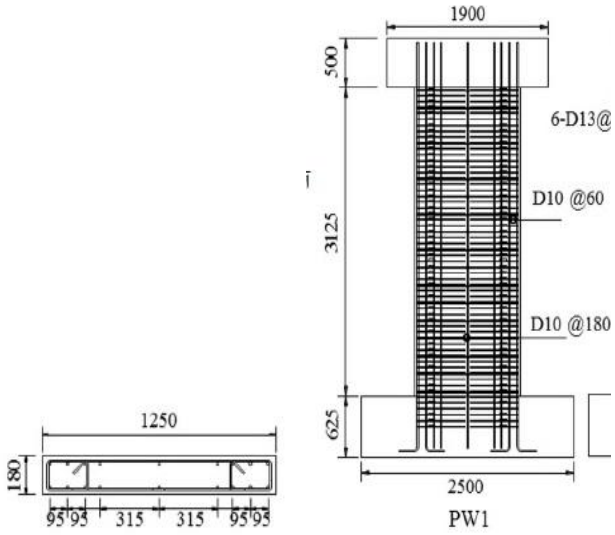


Fig. 5 Dimensions and reinforcement of test specimens

## 3. Finite element simulation

The influence of considered parameters on the length of plastic hinge of the pier wall was evaluated by numerical simulation executed based on the finite element method (FEM) implemented in ABAQUS software. For this aim, the experimental test performedby Seo *et al.* (Seo *et al.* 2017) was adopted for the model apprising. In the considered test programafull scale reinforced concrete wall pier was subjected to cyclic loads provided by prescribing incremental lateral displacement cycles, while the axial load kept constant. Geometrical properties of the wall and reinforcing scheme are represented in Fig.5 and detailed in Table 2.

In the FEM simulation, the 8-node C3D8R cubic element was utilized for three-dimensional modeling of concrete with or without steel reinforcements (Fig. 6). The most important characteristic of this element is its nonlinear material properties. This element has the potential for cracking (in three directions perpendicular to each other), crushing, plastic deformations, and creep. The strain

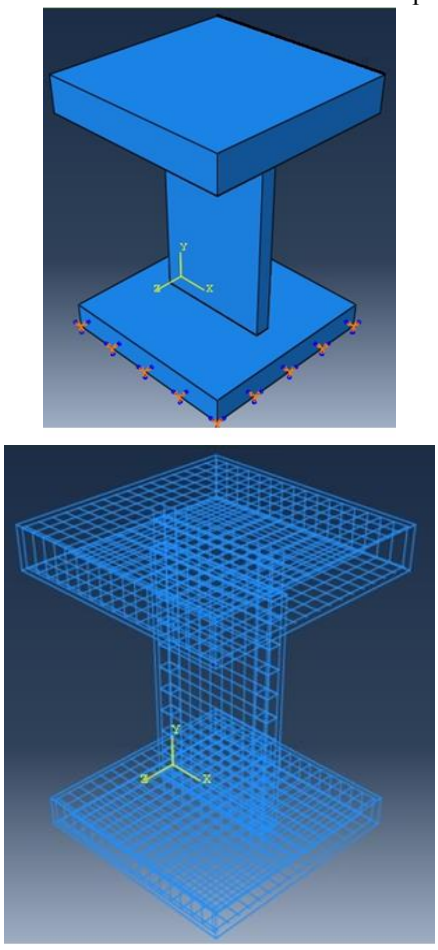

Fig. 6 Finite element modeling of the pier wall in ABAQUS software

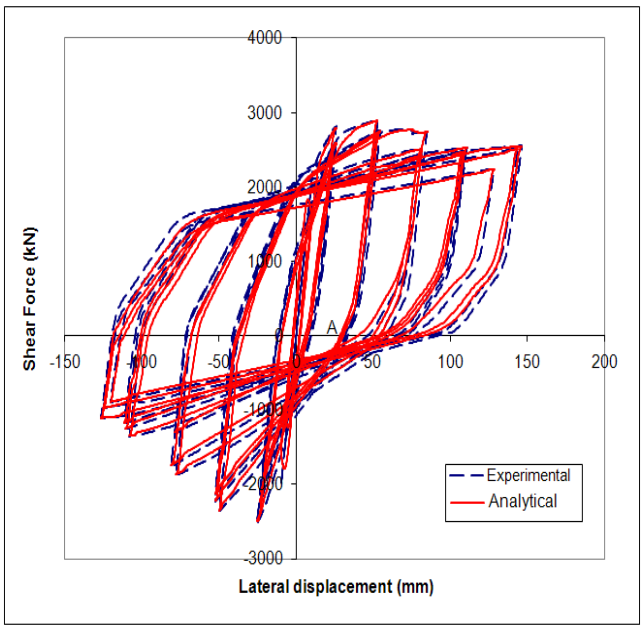


Fig. 7 Hysteresis curvature of shear force-lateral displacement of the wall pier

hardening bar element was also used to model steel reinforcements. This three-dimensional element had two nodes and three degrees of freedom per node. This element can experience the plastic deformation.

The purpose of comparing the finite element model and experimental tests was to ensure the proper performance of the elements, material properties, real constants, and convergence criteria in the numerical modeling of the wall pier. The hysteresis curve of the shear force-lateral displacement of the pier can be observed in Figure 7 in both analytical and experimental conditions, according to which, the high accuracy of the model prediction is revealed. In fact, the FEM simulation can accurately predict the ultimate lateral strength, permanent displacements, stiffness of cracking limit, and energy dissipation. The maximum load and corresponding lateral displacement of 2854.2 kN and 145 mm, respectively, was determined by the FEM simulation, which are desirably closed to the ones determined in experimental program (maximum load of 2793.3kN and corresponding lateral displacement of 141.4).

## 4. Sensitivity analysis

The purpose of the sensitivity analysis in the framework of structural engineering is to examine the performance variability of a structure or a structural element by changing the uncertainty parameters. For estimating the capacity of a structural member, structural analysis includes many assumptions related to the parameters leading to a large degree of uncertainty. The uncertainty arises from the changes in the independent variables may associate with material characteristics and geometric properties known as “epistemic uncertainty”. Therefore, in order to consider the variability or uncertainty associated with random variables, a probabilistic framework is required to evaluate the structural response. Such a probabilistic assessment is obtained through sensitivity analysis, which is considered as an intermediate step in the uncertainty analysis. It is performed with the purpose of identifying the input variables with the greatest effect on the structural response (Celarec and Dolšek 2013). The effect of uncertainty of input parameters on the sensitivity of response parameters has been studied in steel frames (Vamvatsikos and Fragiadakis 2010, Zona *et al.* 2012), masonry buildings (Rota *et al.* 2012), reinforced concrete frames, gravity dams, and bridges (Padgett and DesRoches 2007), and offshore structures (Eldin and Kim 2016).

Porter *et al.* (Porter *et al.* 2002) as well as Celik and Ellingwood (Celik and Ellingwood 2010) used the tornado diagram analysis (TDA) method for seismic sensitivity analysis in estimating the damage to reinforced concrete structures. Seo and Linzell (Seo and Linzell 2013) studied the response sensitivity of a curved steel bridge to various parameters using tornado diagram analysis. Baker and Cornell (2008) employed the first-order second moment (FOSM) method to predict the damage to structures in sensitivity analysis. Lee and Mosalam (2005) examined the sensitivity of the seismic demand to shear wall reinforced concrete structures using the first-order second moment method. They also used different sensitivity analysis methods to estimate the design parameters sensitive to seismic response of buildings. The results of the research work suggested that the first-order second moment can be used with the same level of precision as Monte Carlo simulation for sensitivity analysis of structures.

Accordingly, three different methods of Tornado Diagram Analysis (TDA), First-Order Second Moment (FOSM), and Monte Carlo simulation method (MCS) are used in this paper for sensitivity analysis in order to identify important parameters in determining the characteristics and length of plastic hinge region of RC wall piers. Through sensitivity analysis, uncertainties associated with material properties, geometry, and loading are considered to determine the parameters affecting the properties of the plastic hinge region.

### *4.1 Monte Carlo Simulation (MCS)*

Monte Carlo simulation is one of the most widely used methods for analyzing random problems. In this method, random variables are represented by a group of definite values which are used to generate a group of definite outputs. Then, the probabilistic forms of output are constructed. Because of the precision and strength of this method, MCS is often used to evaluate other probabilistic analysis methods (Lee and Mosalam 2006).

### *4.2 Tornado (swing) analysis*

Tornado diagrams, also called “tornado charts” or “tornado graphs” or “swing tornadoes”, constitute a probabilistic sensitivity analysis method used in decision analysis to estimate the effect of different random variables on response parameters. These diagrams visualize the results of the sensitivity analysis of independent variables (Figure 8). These diagrams were initially developed for

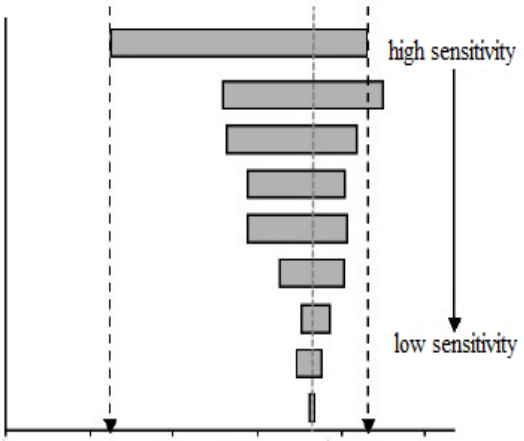


Fig. 8 Schematic representation of tornado diagrams

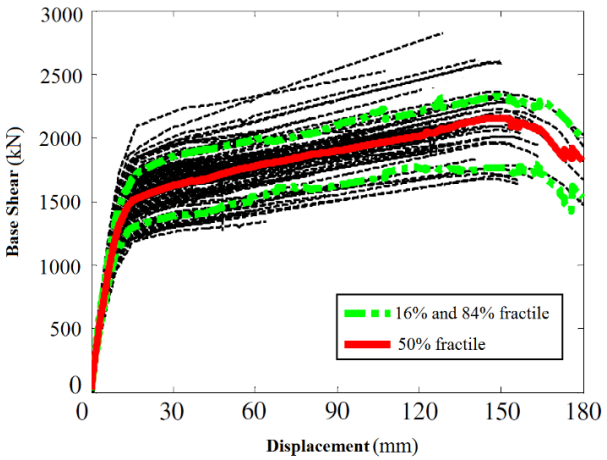


Fig. 9 The sensitivity of the analytical push curves to non-deterministic parameters

financial applications, but they have also been used in structural problems in recent years (Na *et al*. 2008, Baynes 2005, Crozet *et al*. 2018). In this paper, tornado diagrams are used to identify the relative importance of non-deterministic model parameters in estimating the properties of plastic hinge region.

In the tornado analysis, each parameter accepts different values, while other variables are considered constant in their mean values. Two upper and lower values are used to estimate such variations. Moreover, a probabilistic distribution has been assumed for each variable with two percentiles selected which can be 10th and 90th (to achieve a larger sampling) or 16th and 84th (approximately μ-σ and μ + σ of the Gaussian distribution), both of which have been used in this paper.

### *4.3 First-order second moment (FOSM) analysis*

The first-order second moment (FOSM) method is an approximate technique used in the probability theory to find the mean and standard deviation of an output variable using the input variable information (mean, standard deviation, and correlation coefficients) (Lee and Mosalam 2004). In other words, the problem to be solved is as follows:

$$y = g(x_1, x_2, \dots, x_N) = g(x) \tag{1}$$

Where, y is a function of different random variables of $x_i$. By determining the values of VC[x] and $\mu_x$, the mean and variance matrices and the covariance of input values, $\mu_y$ and $\sigma_y$, the mean and standard deviation of the y function must be found. The FOSM estimation does not consider the distribution functions of input variables. This estimation is based on the Taylor series expansion of response function of g around the mean values. Indeed, provided that the deviations of g [x] are available with respect to x, the expansion of the Taylor series g [x] in $\mu_x$ is as follows:

$$y = g(\mu_{x_1}, \mu_{x_2}, \dots, \mu_{x_N}) + \cdots \tag{2}$$

Considering only the first-order sentences of the equation above, i.e., neglecting higher-order sentences, the function y is estimated as follows:

$$y \approx g(\mu_{x_1}, \mu_{x_2}, \dots, \mu_{x_n}) + \cdots \tag{3}$$

By calculating the expected value of both sides, the mean of the function y, $\mu_y$ is expressed as:

$$\mu_y \approx g(\mu_{x_1}, \mu_{x_2}, \dots, \mu_{x_n}) \tag{4}$$

Using the second moment y expressed in Equation (3) and with simplification, the variance of the function y,$\sigma_y^2$ is extracted:

$$\sigma_y^2 \approx \sum_{i=1}^{N} \sum_{j=1}^{N} CoV(x_i, x_j) \frac{\delta g(x_1, x_2, \dots, x_N)}{\delta x_i} \tag{5}$$

Where, $\rho_{x_i x_j}$ represents the correlation coefficient for random values $x_j$and$x_i$; so further numerical analysis is required. The seventeen selected non-deterministic parameters used for the sensitivity analysis are summarized in Table 3.

## 5. Results and discussion

Uncertainty quantification and propagation is examined by uncertainty analysis throw selected samples. Hereupon, random pushover curves are generated by performing analyses for each structural model as shown in Fig. 9.

The results of pushover analyses, which were developed for a wide range of variables, show a significant variation in energy dissipation capacity and base shear force. As can be seen in Fig. 9, the maximum values of base shear forces are varying within the interval between 1400kN and 2850kN. These evaluations highlight the noteworthy effects of structural uncertainties on the bearing and energy dissipation capacity. Therefore, it is very important to examine the random nature and contribution of effective parameters in plastic hinge studies.

It can be seen that the disparity of pushover curves is very small firstly, whereas it is increased rapidly with the increase of the lateral displacement. At the large lateral displacements, the changes are very high. Such a high level

Table 3 Statistical characteristics of the selected variables

| | Uncertain parameter | Symbol | mean | Dimension | COV | Distribution | Authors |
|---|---|---|---|---|---|---|---|
| 1 | Axial load level | $\left(P/P_o\right)$ | 0.4 | - | 0.1 | Log normal | Elingwood *et al.* |
| 2 | aspect ratio | $\left(H/L\right)$ | 4 | - | 1.5 | Log normal | Lee and Mosalam |
| 3 | concrete strength | $(f_c)$ | 25 | MPa | 0.18 | Normal | Elingwood *et al.* |
| 4 | maximum compressive strain of concrete | $(\varepsilon_{c_o})$ | 0.002 | - | 0.285 | Normal | Elingwood *et al.* |
| 5 | maximum tensile strain of concrete | $(\varepsilon_t)$ | 0.00015 | - | 0.285 | Normal | Elingwood *et al.* |
| 6 | concrete tensile strength | $(f_t)$ | 2.5 | MPa | 0.18 | Normal | Elingwood *et al.* |
| 7 | modulus of elasticity of concrete | $(E_c)$ | 24274 | MPa | 0.077 | Normal | Mirza & MacGregor |
| 8 | longitudinal steel yield strength | $(f_{yL})$ | 450 | MPa | 0.093 | Beta | Mirza & MacGregor |
| 9 | transverse steel yield strength | $(f_{ys})$ | 350 | MPa | 0.093 | Beta | Mirza & MacGregor |
| 10 | longitudinal steel ratio | $(\rho_{sL})$ | 0.03 | - | 0.04 | Log normal | Mirza & MacGregor |
| 11 | transverse steel ratio | $(\rho_{sh})$ | 0.02 | - | 0.04 | Log normal | Mirza & MacGregor |
| 12 | ultimate longitudinal steel strain | $(\varepsilon_{ul})$ | 0.01 | - | 0.173 | Normal | Mirza & MacGregor |
| 13 | ultimate strength of the longitudinal steel | $(f_{ul})$ | 650 | MPa | 0.08 | Beta | Mirza & MacGregor |
| 14 | modulus of elasticity of steel | $(E_s)$ | 200000 | MPa | 0.033 | Normal | Mirza & MacGregor |
| 15 | ultimate strain of the transverse steel | $(\varepsilon_{uh})$ | 0.015 | - | 0.173 | Normal | Mirza & MacGregor |
| 16 | longitudinal steel diameter | $(d_{sl})$ | 20 | mm | 0.145 | Normal | Lee and Mosalam |
| 17 | transverse steel diameter | $(d_{sh})$ | 10 | mm | 0.145 | Normal | Lee and Mosalam |

of variability discloses that it is irrational and risky to neglect the effect of structural uncertainties in plastic hinge analysis. Because this can underestimate the potential plastic hinge length conditioned on large deformation.

As the aim of sensitivity analysis is to examine the performance variability of the wall piers under the uncertain parameters, the random variables are characterized by three levels: the base value and the upper and lower limits corresponding to the means and 1 SD beyond and below the means, respectively.

That means the sensitivity analyses are performed independently by testing each non-deterministic parameter with 1 SD above or below its mean. Then, the sensitivity of the cyclic analysis is evaluated, with the backbone curves of these analyses demonstrated in Figure 10. In this figure, the curve with the mean parameters appears as a black line (solid line), while the curves corresponding to the upper and lower limits parameters are dispersed around its sides. This process was performed for various curves such as moment-curvature, lateral force-displacement, backbone curve, cumulative dissipated energy-cycle, yielding area length-cycle. Because of limitation in paper length, only the results of backbone curves are presented.

As shown in Figure 10, the parameters of H/L, $P/P_0$, $\rho_{sl}$, $f_c$ and $f_{yl}$ have quite large effects, while the rest of parameters show very low influences as these three curves are nearly undistinguishable. The results show that the aspect ratio have remarkable effects on the cyclic analysis results as shown in Figs. 10(a). Compared with H/L, the axial load level ($P/P_0$) shows less influence. It is clear that $f_{yl}$ has weighty effects initially. However, its effects decrease with increasing displacement until peak lateral force, in which the response is controlled by ultimate strength of the reinforcement $f_{ul}$. As shown in Fig. 10, the effects of $f_{ul}$ more confirm the response.

Furthermore, the lateral reinforcement $\rho_{sh}$ and the modulus of elasticity of concrete and steel also show good influences. Some of the remaining parameters show clear effects on the final deformation capacity of the wall piers. For example, increasing the strain-related parameters εt and εul to 1 SD above the means could increase the final lateral displacement of wall piers meaningfully.

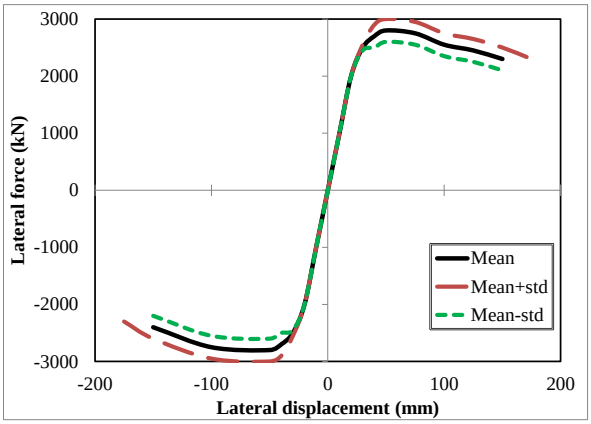

(a)

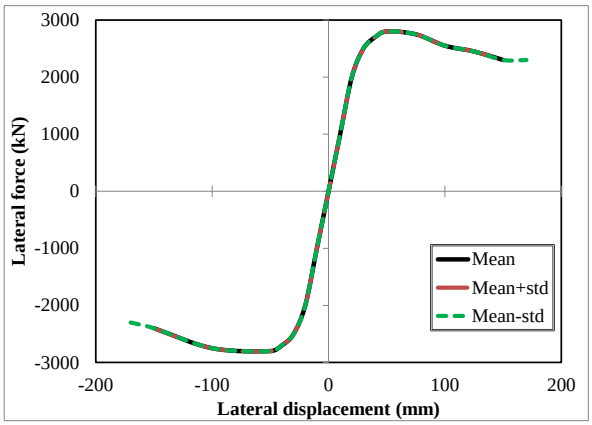
Lateral force (kN)
3000
2000
1000
0
-1000
-2000
-3000
-200
-100
0
100
200
Lateral displacement (mm)
Mean
Mean+std
Mean-std

(b)

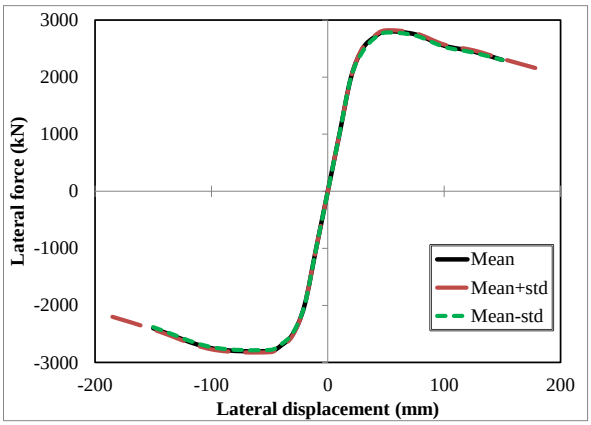
Lateral force (kN)
3000
2000
1000
0
-1000
-2000
-3000
-200
-100
0
100
200
Lateral displacement (mm)
Mean
Mean+std
Mean-std

(f)

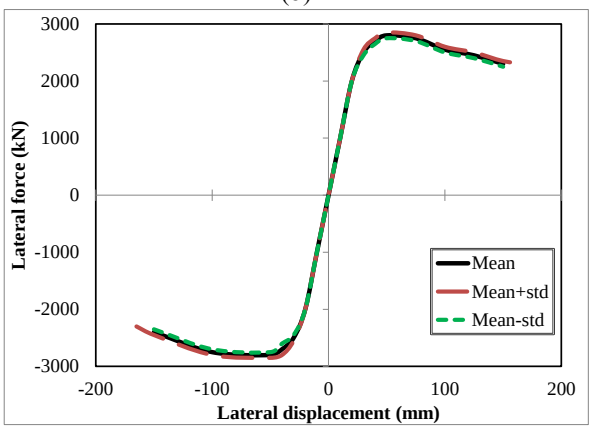
Lateral force (kN)
3000
2000
1000
0
-1000
-2000
-3000
-200
-100
0
100
200
Lateral displacement (mm)
Mean
Mean+std
Mean-std

(c)

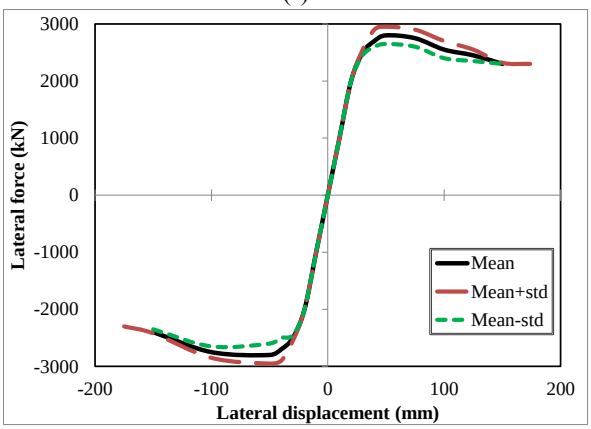
Lateral force (kN)
3000
2000
1000
0
-1000
-2000
-3000
-200
-100
0
100
200
Lateral displacement (mm)
Mean
Mean+std
Mean-std

(g)

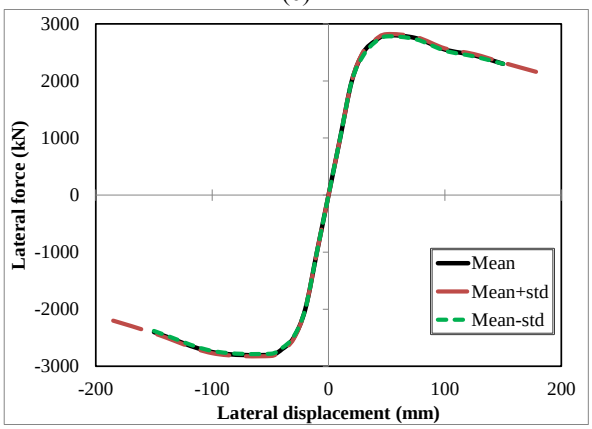
Lateral force (kN)
3000
2000
1000
0
-1000
-2000
-3000
-200
-100
0
100
200
Lateral displacement (mm)
Mean
Mean+std
Mean-std

(d)

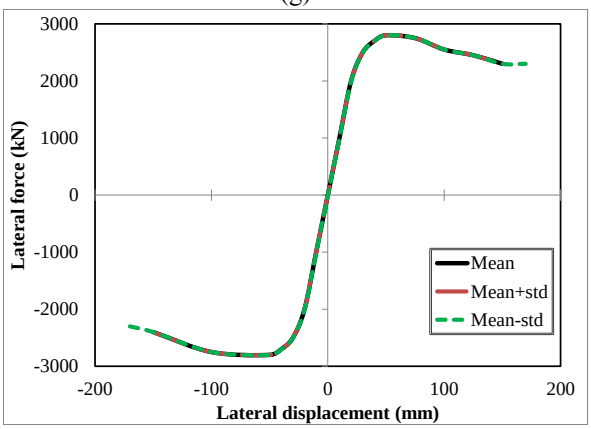
Lateral force (kN)
3000
2000
1000
0
-1000
-2000
-3000
-200
-100
0
100
200
Lateral displacement (mm)
Mean
Mean+std
Mean-std

(h)

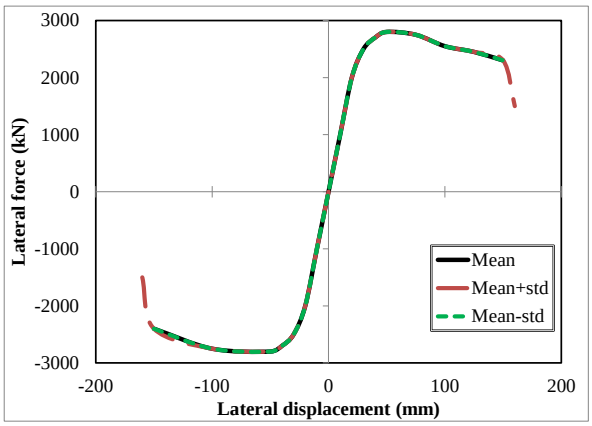
Lateral force (kN)
3000
2000
1000
0
-1000
-2000
-3000
-200
-100
0
100
200
Lateral displacement (mm)
Mean
Mean+std
Mean-std

(e)

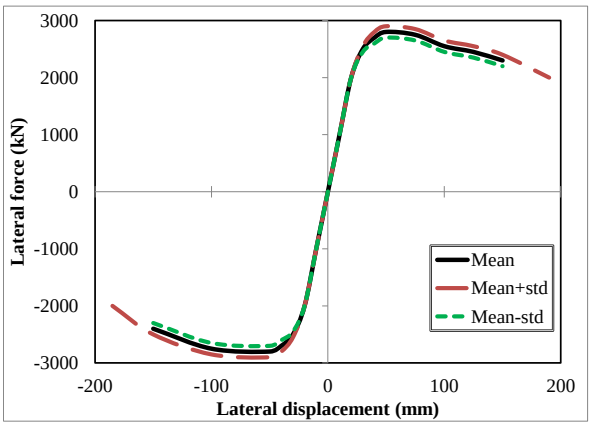
Lateral force (kN)
3000
2000
1000
0
-1000
-2000
-3000
-200
-100
0
100
200
Lateral displacement (mm)
Mean
Mean+std
Mean-std

(i)

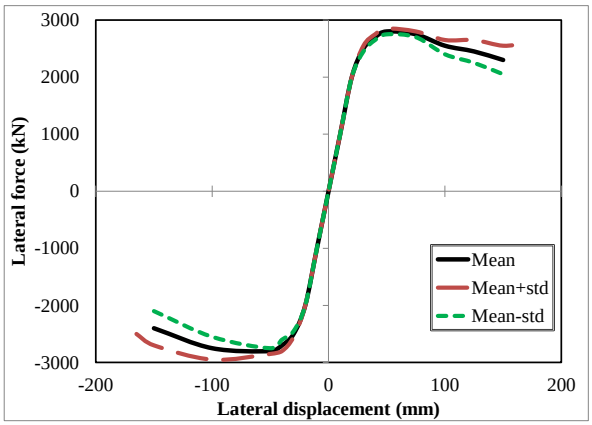
Lateral force (kN)
3000
2000
1000
0
-1000
-2000
-3000
-200
-100
0
100
200
Lateral displacement (mm)
Mean
Mean+std
Mean-std

(j)

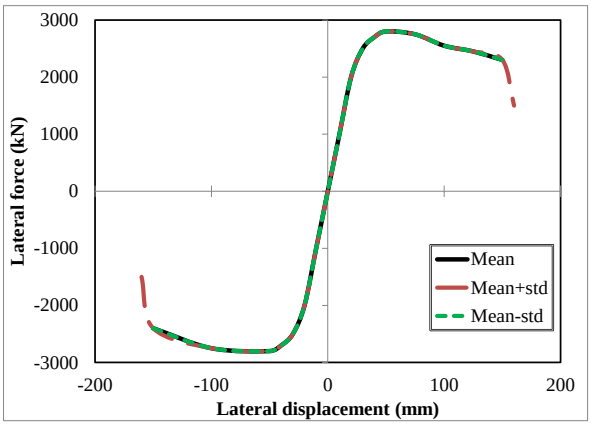
Lateral force (kN)
3000
2000
1000
0
-1000
-2000
-3000
-200
-100
0
100
200
Lateral displacement (mm)
Mean
Mean+std
Mean-std

(n)

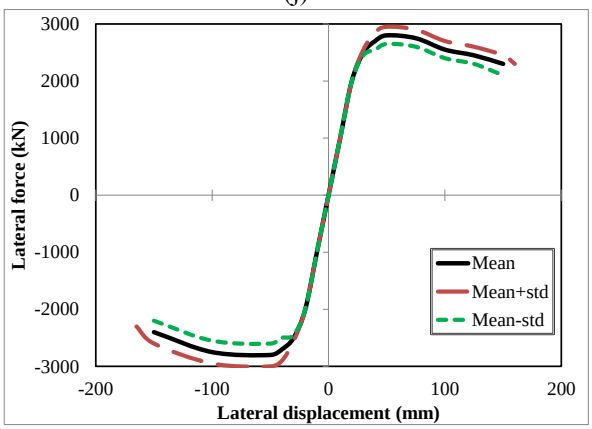
Lateral force (kN)
3000
2000
1000
0
-1000
-2000
-3000
-200
-100
0
100
200
Lateral displacement (mm)
Mean
Mean+std
Mean-std

(k)

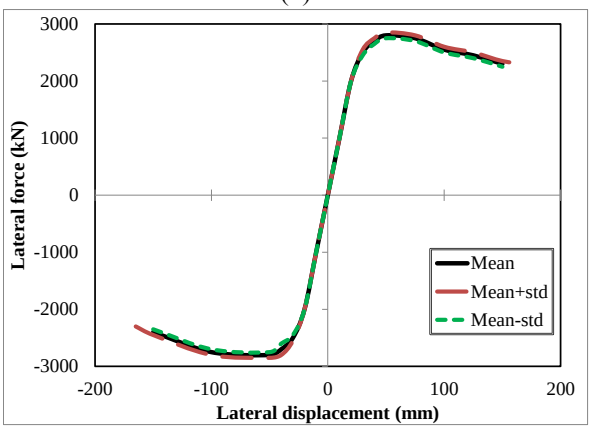
Lateral force (kN)
3000
2000
1000
0
-1000
-2000
-3000
-200
-100
0
100
200
Lateral displacement (mm)
Mean
Mean+std
Mean-std

(o)

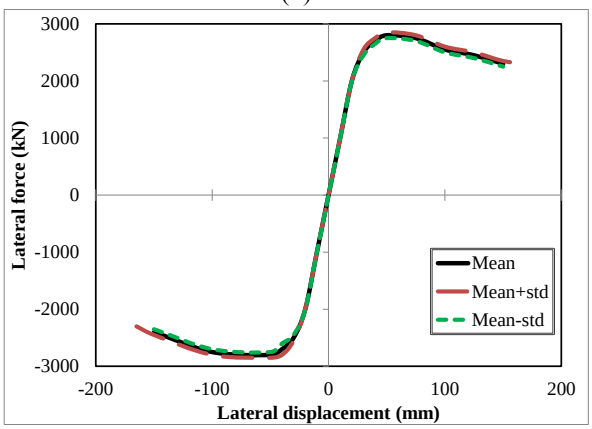
Lateral force (kN)
3000
2000
1000
0
-1000
-2000
-3000
-200
-100
0
100
200
Lateral displacement (mm)
Mean
Mean+std
Mean-std

(l)

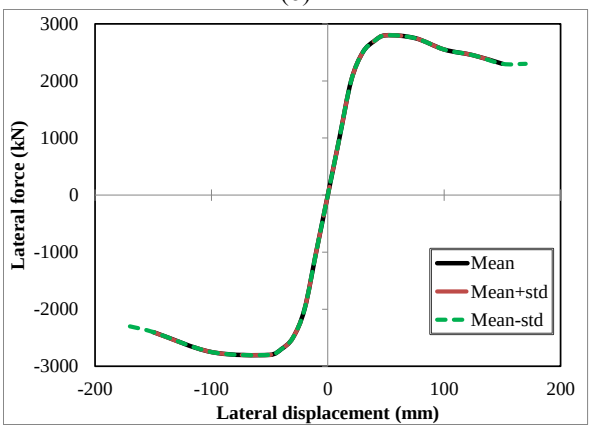
Lateral force (kN)
3000
2000
1000
0
-1000
-2000
-3000
-200
-100
0
100
200
Lateral displacement (mm)
Mean
Mean+std
Mean-std

(p)

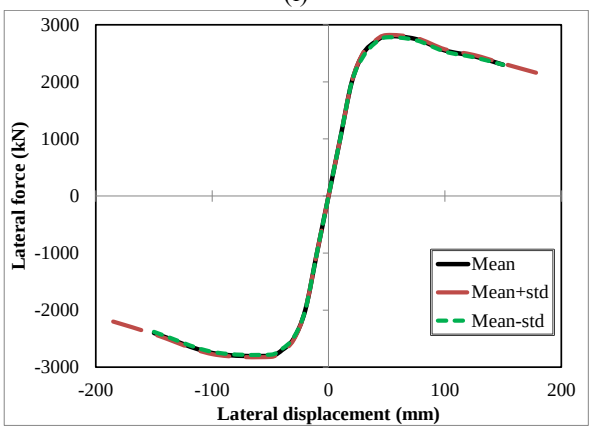
Lateral force (kN)
3000
2000
1000
0
-1000
-2000
-3000
-200
-100
0
100
200
Lateral displacement (mm)
Mean
Mean+std
Mean-std

(m)

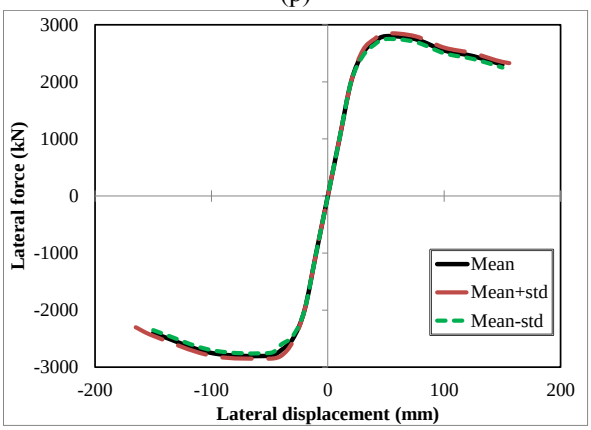
Lateral force (kN)
3000
2000
1000
0
-1000
-2000
-3000
-200
-100
0
100
200
Lateral displacement (mm)
Mean
Mean+std
Mean-std

(q)

Fig. 10. Sesitivity of the backbone curves to the selected uncertain parameters: (a) H/L; (b) $f_t$; (c) $f_c$; (d) $\varepsilon_t$; (e) $E_s$; (f) $\varepsilon_{ul}$; (g) $f_{yl}$; (h) $\varepsilon_{c_o}$; (i) $\rho_{sl}$; (j) $f_{ul}$; (k) $P/P_0$; (l) $\rho_{sh}$; (m) $d_{sl}$; (n) $\varepsilon_{uh}$; (o) $E_c$; (p) $f_{ys}$; (q) $d_{sh}$

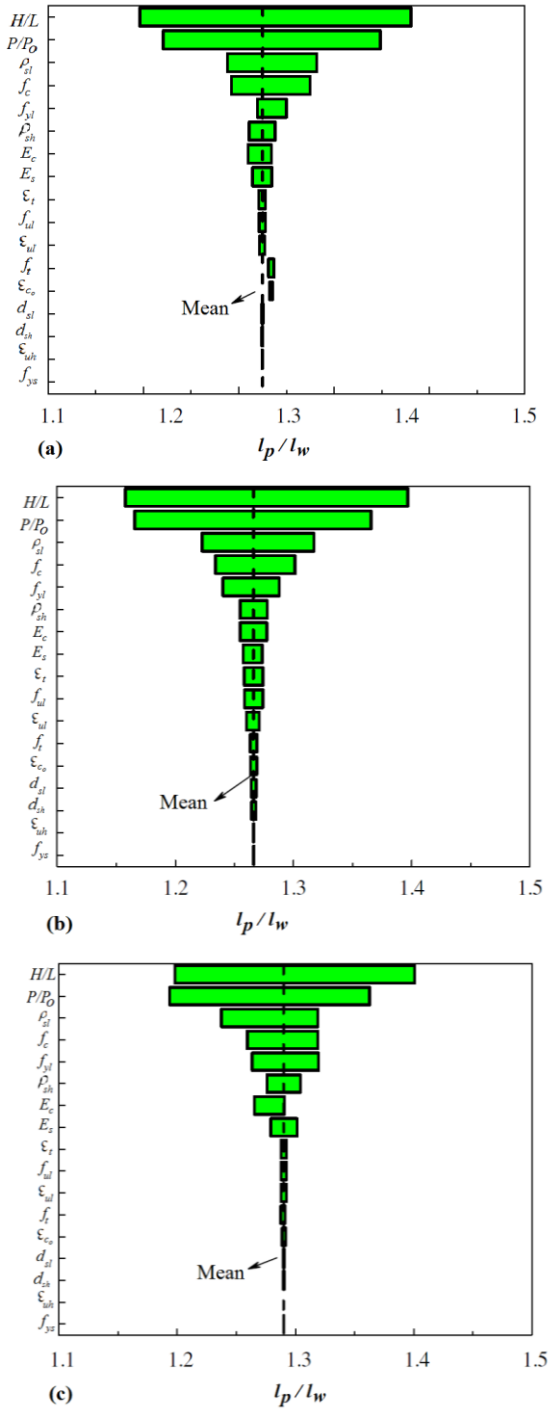


Fig. 11 Tornado diagrams for the samples examined based on (a) TDA, (b) MCS, and (c) FOSM

The sensitivity of each indeterminate parameter on plastic hinge length is examined by the tornado diagrams. In tornado diagram, fluctuations due to different random variables are arranged in descending order and based on the

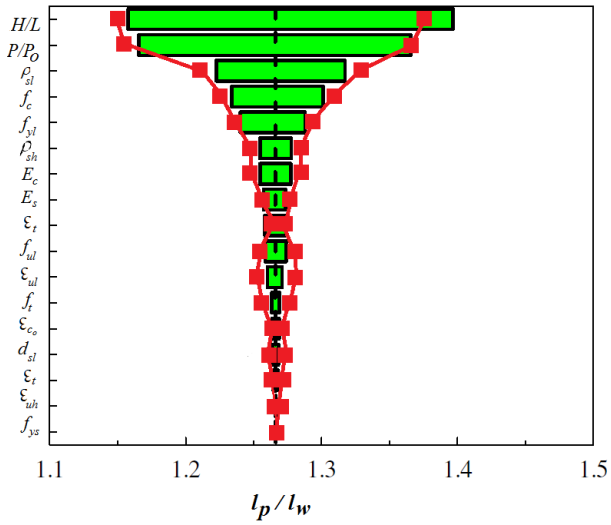


Fig. 12 Tornado diagram of plastic region length along with swinging chart derived from FOSM analysis

fluctuation size from top to bottom. The fluctuation with a larger width means the greater effect of the random variable associated with the length of the plastic region. In order to compare sensitivity based on three different methods, the results of MCS and FOSM methods are also shown in the form of tornado diagrams. Accordingly, the sensitivity of each non-deterministic parameter to the length of the plastic region is investigated through tornado diagrams, with its results shown in Figure 11. As shown in these diagrams, the axial load level $\left(P/P_o\right)$ and the aspect ratio $\left(H/L\right)$ are parameters whose importance is completely evident in determining the length of the plastic region. Also, the effect of the parameters $\rho_{sL}$ and $f_c$ is also significant.

Figure 11 shows that the variables $P/P_o$, $H/L$, $\rho_{sL}$, $f_c$,$f_{yL}$and $\rho_{sh}$ have almost the maximum effects, while the influence of the remains is marginal. According to Fig. 11, the axial load level and height-to-length ratio had a great influence on the length of the plastic region.

An interesting comparison can be made between the results of the tornado diagrams and the FOSM results. This can be done by assuming a log-normal distribution of the length of the plastic region with the mean value and standard deviations obtained from the FOSM results. Hence, 10th and 90th percentiles can be determined. The resulting values are the points given in Figure 12 and displayed on the bars of the tornado diagrams.

Adequate consistency has been achieved between the two methods. However, it should be reminded that the corners of each oscillating axis in the tornado diagrams are not necessarily 10% and 90% percentiles, unless the relationship between the length of the plastic region and the random variable is monotonic; this monotonic mode is true for the FOSM method. It is worth noting that the order of the significance of different variables is different in two different methods, which is related to the characteristics of the variables concerned, which has little effect on the plastic region length.

## 6. Conclusion

Considering the importance of the length of plastic hinge region in the seismic behavior of wall piers of the reinforced concrete bridges, in this paper, the effect and significance of the random nature of the variables of loading, geometry, and properties of concrete and steel materials were investigated through uncertainty and sensitivity analysis. Three methods of Monte Carlo simulation, tornado diagram, and first-order second moment were employed in this study. Seventeen non-deterministic parameters were selected as random variables which can be classified into four groups: material properties of concrete, material properties of steel, loading level, and member geometry. All three adopted methods had almost the same ranking for weighting the importance of effective parameters.

Disparity of pushover curves was very small initially, while it was increased rapidly with the increase of the lateral displacement. At the large lateral displacements, the changes was very high; as it was increased to about twice as much. Such a high level of variability discloses that it is unreasonable to neglect the effect of structural uncertainties in plastic hinge analysis.

It was revealed that the uncertainties associated with loading, geometry, and material properties of materials had the greatest relationship. In particular, the pier wall aspect ratio (H/L), the axial load level ($P/P_0$), the concrete strength ($f_c$), the percentage of longitudinal steel ($\rho_{sl}$), and the yield strength of longitudinal reinforcement ($f_{yl}$) play an important role in the properties of the plastic hinge region.

Yield strength of longitudinal reinforcement ($f_{yl}$) had weighty effects initially. However, its effects decrease with increasing displacement until peak lateral force, in which the response is controlled by the ultimate strength of longitudinal reinforcement ($f_{ul}$).

## References


AASHTO (2011), *Guide Specifications for LRFD Seismic Bridge Design*, American Association of State Highway and Transportation Officials, Washington, D.C., USA.

ACI Committee 318 (2014), *Building Code Requirements for Structural Concrete (ACI 318-14) and Commentary (ACI 318R-14)*, American Concrete Institute; Farmington Hills, Michigan, USA.

Alembagheri, M. and Seyedkazemi, M. (2015), "Seismic performance sensitivity and uncertainty analysis of gravity dams", *Earthq. Eng. Struct. Dynam.*, **44**(1), 41–58. https://doi.org/10.1002/eqe.2457.

Alim, H. (2014), "Reliability based seismic performance analysis of retrofitted concrete bridge bent", M.Sc. Disseration, Chittagong University of Engineering and Technology (CUET), Chittagong, Bangladesh.

Aslani, H., Cabrera, C. and Rahnama, M. (2012), "Analysis of the sources of uncertainty for portfolio-level earthquake loss estimation", *Earthq. Eng. Struct. Dynam*., **41**(11), 1549-1568. https://doi.org/10.1002/eqe.2230.

Baker, J.W. and Cornell, C.A. (2008), "Uncertainty propagation in probabilistic seismic loss estimation", *Struct. Safety*, **30**(3), 236–252. https://doi.org/10.1016/j.strusafe.2006.11.003.

Baynes, L.C. (2005), "An evaluation of free field liquefaction analysis using OpenSees", M.Sc. Dissertation, University of Washington, Seattle, USA.

Caltrans (2013), *Seismic Design Criteria 1.7*., California Department of Transportation; Sacramento, CA, USA.

Canadian Standard Association (2004), *Design of Concrete Structures*, *CAN/CSA-A23.3-04*, Mississauga, Ontario, Canada.

Celarec, D. and Dolšek, M. (2013), "The impact of modelling uncertainties on the seismic performance assessment of reinforced concrete frame buildings", *Eng. Struct.*, **52**, 340–354. https://doi.org/10.1016/j.engstruct.2013.02.036.

Celik, O.C. and Ellingwood, B.R. (2010), "Seismic fragilities for nonductile reinforced concrete frames - Role of aleatoric and epistemic uncertainties", *Struct. Safety*, **32**(1), 1–12. https://doi.org/10.1016/j.strusafe.2009.04.003.

CEN (2004), *Eurocode 8: Design of Structures for Earthquake Resistance. Part 1: General Rules, Seismic Actions and Rules for Buildings, EN 1198-1*, European Committee for Standardization; Belgium.

CEN (2005), *Eurocode 8: design provisions of structures for earthquake resistance. Part 2: Bridges. EN 1998-2*. European Committee for Standardization; Belgium.

Crozet, V., Politopoulos, I., Yang, M., Martinez, J.M. and Erlicher, S. (2018), "Sensitivity analysis of pounding between adjacent structures", *Earthq. Eng. Struct. Dynam*., **47**(1), 219–235. https://doi.org/10.1002/eqe.2949.

Eldin, M.N. and Kim, J. (2016), "Sensitivity analysis on seismic life-cycle cost of a fixed-steel offshore platform structure", *Ocean Eng.*, **121**, 323–340. https://doi.org/10.1016/j.oceaneng.2016.05.050.

Ellingwood, B., Galambos, T.V., MacGregor, J.G. and Cornell, C.A. (1980), *Development of a Probability Based Load Criterion for American National Standard A58—Building Code Requirement for Minimum Design Loads in Buildings and Other Structures*, National Bureau of Standards, Dept. of Commerce, Washington, D.C., USA.

Ghaderi Bafti, F., Mortezaei, A. and Kheyroddin, A. (2019), "The length of plastic hinge area in the flanged reinforced concrete shear walls subjected to earthquake ground motions", *Struct. Eng. Mech.*, **69**(6), 651-665. http://dx.doi.org/10.12989/sem.2019.69.6.651.

Lee, T.H. and Mosalam, K.M. (2004), "Probabilistic fiber element modeling of reinforced concrete structures", *Comput. Struct.*, **82**, 2285–2299. https://doi.org/10.1016/j.compstruc.2004.05.013.

Lee, T.H. and Mosalam, K.M. (2005), "Seismic demand sensitivity of reinforced concrete shear-wall building using FOSM method", *Earthq. Eng. Struct. Dynam.*, **34**(14), 1719–1736. https://doi.org/10.1002/eqe.506.

Lee, T.H. and Mosalam, K.M. (2006), "Probabilistic Seismic Evaluation of Reinforced Concrete Structural Components and Systems", University of California, Berkeley, CA, USA.

Management and Planning Organization (2005), *Road Safety Manual: Safety at Bridge and Tunnel, No: 267*, Office of Deputy for Technical Affairs, Technical, Criteria Codification and Earthquake Risk Reduction Affairs Bureau, Tehran, Iran.

Ministry of Roads and Transportation (2008), *Road and Railway Bridges Seismic Resistant Design Code, NO: 463*, Office of Deputy for Strategic Supervision Bureau of Technical Execution System, Ministry of Roads and Transportation, Tehran, Iran.

Mirza, S.A. and MacGregor, J.G. (1979), "Variability in dimensions of reinforced concrete members", *J. Struct. Division*, **105**(ST4), 751–766.

Mirza, S.A. and MacGregor, J.G. (1979), "Variability of mechanical properties of reinforcing bars", *J. Struct. Division*, **105**(ST5), 921–937.

Mortezaei, A. (2015), "Effect of frequency content of near-fault ground motions on seismic performance of reinforced concrete bridge piers", *J. Transport. Infrastruct. Eng.*, **1**(3), 93-109.

Mortezaei, A. and Ronagh, H.R. (2012), "Plastic hinge length of

FRP strengthened reinforced concrete columns subjected to both far-fault and near-fault ground motions", *Scientia Iranica*, **19**, 1365–1378.

Murat, O. (2015), "Field Reconnaissance of the October 23, 2011, Van, Turkey Earthquake: Lessons from Structural Damages", *J. Performance Construct. Facilities*, **29**(5), https://doi.org/10.1061/(ASCE)CF.1943-5509.0000532.

Na, U.J., Chaudhuri, S.R. and Shinozuka, M. (2008), "Probabilistic assessment for seismic performance of port structures", *Soil Dynam. Earthq. Eng.*, **28**(2),147-158.

NZS 3101 (2006), *The Design of Concrete Structures. Concrete Structures Standard, Part 1: Code of practice*, Wellington, New Zealand Standard, New Zealand.

Padgett, J.E. and DesRoches, R. (2007), "Sensitivity of seismic response and fragility to parameter uncertainty", *J. Struct. Eng.*, **133**(12), 1710-1718. https://doi.org/10.1061/(ASCE)0733-9445(2007)133:12(1710).

Porter, K.A., Beck, J.L. and Shaikhutdinov, R.V. (2002), "Investigation of sensitivity of building loss estimates to major uncertain variables for the Van Nuys test bed", Pacific Earthquake Engineering Research Center, University of California, Berkeley, USA.

Rota, M., Penna, A. and Magenes, G. (2010), "A methodology for deriving analytical fragility curves for masonry buildings based on stochastic nonlinear analyses", *Eng. Struct.*, **32**(5), 1312–1323. https://doi.org/10.1016/j.engstruct.2010.01.009.

Seo, J. (2013), "Statistical determination of significant curved I-girder bridge seismic response parameters", *Earthq. Eng. Eng. Vib.*, **12**(2), 251–260. https://doi.org/10.1007/s11803-013-0168-y.

Seo, J. and Linzell, D.G. (2013), "Nonlinear seismic response and parametric examination of horizontally curved steel bridges using 3D computational models", *J. Bridge Eng.*, **18**(3), 220–231. https://doi.org/10.1061/(ASCE)BE.1943-5592.0000345.

Seo, M.S., Kim, H.S., Truong, G.T. and Choi, K.K. (2017), "Seismic behaviors of thin slender structural walls reinforced with amorphous metallic fibers", *Eng. Struct.*, **152**, 102-115. https://doi.org/10.1016/j.engstruct.2017.09.004.

Sung, Y. C., Chang, D. W., Cheng, M. Y., Chang, T. L. and Liu, K. Y. (2009), "Enhancing the structural longevity of the bridges with insufficient seismic capacity by retrofitting", *Structural Longevity*, **1**(1), 1-16.

Vamvatsikos, D. and Fragiadakis, M. (2010), "Incremental dynamic analysis for estimating seismic performance sensitivity and uncertainty", *Earthq. Eng. Struct. Dynam*, **39**(2), 141–163. https://doi.org/10.1002/eqe.935.

Zona, A., Ragni, L. and Dall'Asta, A. (2012), "Sensitivity-based study of the influence of brace over-strength distributions on the seismic response of steel frames with BRBs", *Eng. Struct.*, **37**, 179–192. https://doi.org/10.1016/j.engstruct.2011.12.026.

*CC*